Spectral Resolution of the Split EPR Signals Induced by Illumination at 5 K from the S_1, S_3, and S_0 States in Photosystem II†

Kajsa G. V. Havelius,‡ Ji-Hu Su,‡,§ Yashar Feyziyev,|| Fikret Mamedov,‡ and Stenbjörn Styring*,‡

Molecular Biomimetics, Department of Photochemistry and Molecular Science, Ångström Laboratory, Uppsala University, P.O. Box 523, S-751 20 Uppsala, Sweden, and Institute of Botany, Patamdar shosse 40, AZ-1073 Baku, Azerbaijan

Received April 11, 2006

ABSTRACT: S-State-dependent split EPR signals that are induced by illumination at cryogenic temperatures (5 K) have been measured in spinach photosystem II without interference from the $Y_D^{\bullet}$ radical in the $g \sim 2$ region. This allows us to present the first decay-associated spectra for the split signals, which originate from the $CaMn_4$ cluster in magnetic interaction with a nearby radical, presumably $Y_Z^{\bullet}$. The three split EPR signals that were investigated, "Split S_1", "Split S_3", and Split S_0", all exhibit spectral features at $g \sim 2.0$ together with surrounding characteristic peaks and troughs. From microwave relaxation studies we can reach conclusions about which parts of the complex spectra belong together. Our analysis strongly indicates that the wings and the middle part of the split spectrum are parts of the same signal, since their decay kinetics in the dark at 5 K and microwave relaxation behavior are indistinguishable. In addition, our decay-associated spectra indicate that the $g \sim 2.0$ part of the "Split S_1" EPR spectrum contains a contribution from magnetically uncoupled $Y_Z^{\bullet}$ as judged from the g value and 22 G line width of the EPR signal. The g value, 2.0033−2.0040, suggests that the oxidation of Y_Z at 5 K results in a partially protonated radical. Irrespective of the S state, a small amount of a carotenoid or chlorophyll radical was formed by the illumination. However, this had relaxation and decay characteristics that clearly distinguish this radical from the split signal spectra. In this paper, we present the "clean" spectra from the low-temperature illumination-induced split EPR signals from higher plants, which will provide the basis for further simulation studies.

Photosystem II (PSII)[1] in the thylakoid membrane of higher plants, algae, and cyanobacteria (*1*) catalyzes the light-driven reduction of plastoquinone using electrons ultimately derived from water. The core of PSII is composed of the D1−D2 reaction center dimer that is surrounded by CP43, CP47, Cyt b_{559}, 11 small subunits, and three extrinsic proteins on the luminal side of the membrane (*2*−*6*). The photon energy is captured by pigments in antenna proteins and directed to primary electron donor P_{680}. Excitation of P_{680} is followed by the primary charge separation giving the P_{680}^{+}pheophytin^{-} charge pair. Pheo^{-} is rapidly oxidized by Q_A and subsequently by electron transfer to Q_B, which after two consecutive reductions and protonation dissociates from PSII. P_{680}^{+} is reduced by a nearby tyrosine residue, Y_Z, which is deprotonated to a nearby base (probably D1-His190) (*7*−*10*), producing the neutral $Y_Z^{\bullet}$ radical. $Y_Z^{\bullet}$ is reduced from the $CaMn_4$ cluster and ultimately from water. The catalytic site for water oxidation is composed of four Mn ions, one Ca^{2+}, and Cl^{-} as a cofactor (*4*, *11*). During water oxidation, it cycles through five intermediate states, S_0−S_4 (*12*). Molecular oxygen is released in the $S_3 \rightarrow [S_4] \rightarrow S_0$ transition. The S_1 state is stable and dominates in the dark-adapted material. S_2 and S_3 are metastable intermediate states that can be studied after one or two flashes given to a sample incubated in the dark. S_0 is the most reduced state and can be produced by subjecting a dark-adapted sample to three flashes.

Under certain conditions, a pathway involving Cyt b_{559}, a Car, and a chlorophyll denoted Chl_Z provides electrons to P_{680}^{+} (*13*−*16*). This also holds true for Y_D, which is situated on the D2 protein in a manner homologous to that of Y_Z (*17*). Y_D is not functional in linear electron transport but participates in charge equilibria with the $CaMn_4$ cluster (*18*, *19*). $Y_D^{\bullet}$ has a very stable radical $g = 2.0046$ EPR spectrum, which facilitates detailed spectroscopic investigations with many techniques (*20*). Y_Z is more difficult to study because of the fast decay and the magnetic interference from the close-lying $CaMn_4$ cluster in intact PSII. Therefore, Y_Z has

† The Swedish Research Council, the Swedish Energy Agency, and the Knut and Alice Wallenberg Foundation are acknowledged for financial support.

* To whom correspondence should be addressed. Phone: +46-18-471 65 80. Fax: +46-18-55 98 85. E-mail: stenbjorn.styring@fotomol.uu.se.

‡ Uppsala University.

§ Current address: Max Planck Institute for Bioinorganic Chemistry, Stiftstrasse 34-36, D-454 70 Mülheim an der Ruhr, Germany.

|| Institute of Botany.

[1] Abbreviations: Car, carotenoid; Chl, chlorophyll; Chl_Z, secondary chlorophyll electron donor to P_{680}^{+}; Cyt b_{559}, cytochrome b_{559}; CP43 and CP47, chlorophyll proteins of 43 and 47 kDa, respectively; D1 and D2, core subunits in PSII; DAD, 3,6-diaminodurene; DMSO, dimethyl sulfoxide; dpa, dipicolylamine; EPR, electron paramagnetic resonance; MES, 4-morpholinoethanesulfonic acid; ML, multiline; NIR, near-infrared; OEC, oxygen-evolving complex; $P_{1/2}$, microwave power to reach half-saturation; P_{680}, primary electron donor of PSII; Pheo, pheophytine; P*p*BQ, phenyl-*p*-benzoquinone; PSII, photosystem II; Q_A and Q_B, primary and secondary quinone acceptors, respectively, in PSII; Y_Z, tyrosine 161 on the D1 subunit; Y_D, tyrosine 161 on the D2 subunit.

10.1021/bi060698e CCC: $33.50
Published on Web 07/11/2006

mostly been studied in Mn-depleted PSII, where the radical lives for 150−700 ms compared to 0.03−1 ms in intact material (*21*, *22*). However, these studies are of limited value in understanding molecular details of Y_Z in the intact system. More functional probes to $Y_Z^\bullet$ are the so-called split EPR signals from the OEC. These were first found in modified PSII depleted of Ca^{2+} or Cl^- or displaced by various treatments (early findings reviewed in ref *23*). By illumination of these samples at 0 °C, a split EPR signal was formed. This was 160 G wide (the width varied with treatment) and centered around $g = 2.0$ (*24*−*40*) and arises from an $S = {}^1/_2$ radical in magnetic interaction with the $CaMn_4$ cluster. The most favored candidate for the radical is $Y_Z^\bullet$ (*30*, *40*−*44*), and the signal was attributed to the $S_2Y_Z^\bullet$ redox state.

The $S_2Y_Z^\bullet$ split signals in inhibited systems have provided much structural and functional information about Y_Z and the $CaMn_4$ cluster. With respect to the *functional* OEC, more information is provided by recently discovered "split signals" that are induced by illumination at cryogenic temperatures (4−20 K) in the S_1 (*45*−*48*) and S_0 states (*46*, *48*). Both the "Split S_1" and "Split S_0" signals can be induced by a single flash at 5 K and oscillate with the respective S state (*46*). The signals have preliminarily been assigned to magnetic interaction between $Y_Z^\bullet$ and the $CaMn_4$ cluster in the respective S state (*45*−*47*, *49*). A signal similar to the "Split S_1" signal can also be formed by NIR illumination (700−900 nm) at 5 K of centers in the S_2 state (*50*). Approximately 50% of the PSII in the S_0 state and 40% in the S_1 state have been found to give rise to the split signals in *Thermosynechococcus elongatus* on the basis of the amount of Q_A^- formed simultaneously during the induction of the split signal (*48*). These numbers are consistent with numbers determined by other indirect methods (*45*, *46*). Thus, the "split-forming pathway" is a dominating pathway during light-induced electron transfer in and around the OEC at cryogenic temperatures.

NIR illumination at 50 K of intact PSII in the S_3 state results in formation of a split $g = 2$ signal. It was proposed that the infrared illumination directly excites the $CaMn_4$ cluster in the S_3 state to a potential sufficiently high to oxidize the nearby Y_Z, and the signal was attributed to magnetic interaction between a modified S_2 state and, most probably, $Y_Z^\bullet$ (*51*−*53*). We study a similar signal induced in a S_3 state with visible light at 5 K.

In this paper, the split EPR signals, originating from the S_1, S_3, and S_0 states, are investigated. These are induced by weak illumination at 5 K of PSII prepared in the different S states with a different number of flashes. Most published spectra of the split signals are obscured by the large EPR signal from the oxidized $Y_D^\bullet$ dominating at $g = 2.00$. Therefore, this spectroscopically important region has often been discarded in published spectra. Two exceptions are the $S_2Y_Z^\bullet$ split signal in Ca^{2+}-depleted PSII and the NIR-induced S_3 signal that recently have been measured in a mutant lacking Y_D in *T. elongatus* (*54*).

Here we study PSII from higher plants (spinach), which is quite different from the cyanobacterial enzyme, in samples where $Y_D^\bullet$ was chemically reduced prior to the EPR measurements. In this way, the spectra from the light-induced split signals could be determined without interference from $Y_D^\bullet$. The first decay-associated spectra for the "Split S_1", "Split S_3", and "Split S_0" signals are presented. This also enables microwave relaxation studies of all three signals that allow us to draw conclusions about which parts of the complex spectra belong together.

MATERIALS AND METHODS

PSII Membrane Preparation. PSII-enriched membranes [BBYs (*55*)] were prepared from hydroponically grown greenhouse spinach (*Spinacia oleracea*) with modifications described in ref *56*. The storage buffer was 25 mM MES-NaOH (pH 6.1), 15 mM NaCl, 3 mM $MgCl_2$, and 400 mM sucrose. Chl determinations were made according to the work of Arnon (*57*). EPR measurements were performed at 2−4 mg of Chl/mL.

Chemical Reduction of Y_D. To prevent EPR subtraction artifacts and a spectral contribution in the $g \sim 2$ region from the large EPR spectrum from $Y_D^\bullet$, $Y_D^\bullet$ was reduced chemically by an ascorbate/DAD treatment in complete darkness (*18*, *58*) to contain only 1.5% $Y_D^\bullet$ (Figure 1A, inset). The PSII particles (at 1.0 mg of Chl/mL) were dark-adapted for 1 h on ice, incubated with a 10 mM ascorbate/3 mM DAD solution for 40 min at 20 °C, and thereafter washed three times in storage buffer at 2 °C to remove the chemical reductants. P*p*BQ [1 mM, dissolved in DMSO, final DMSO concentration of 2% (v/v)] was added to the reduced PSII sample before the EPR tubes were filled in the dark and rapidly frozen. These dark-adapted samples were used to study PSII in the S_1 state.

Steady-State Oxygen Evolution. Steady-state oxygen evolution in saturating light at 20 °C was assessed with a Clark-type electrode (Hansatech Instruments). The Chl concentration was 10 μg of Chl/mL in a buffer with 25 mM MES-NaOH (pH 6.1), 15 mM NaCl, 3 mM $MgCl_2$, and 400 mM sucrose. P*p*BQ (0.5 mM in DMSO) was used as an electron acceptor. The oxygen evolution was 400 ± 50 μmol of O_2 (mg of Chl)$^{-1}$ h^{-1} and remained constant after the reduction protocol and subsequent washings.

Flash Advancement of the S States. The dark-adapted EPR samples with Y_D reduced and containing 0.5 mM P*p*BQ were given two or three saturating flashes at 5 Hz from a Nd:YAG laser (6 ns, 532 nm, 400 mJ/pulse) at 0 °C. After the flashes, the samples were then frozen within 1−2 s. In the presence of reduced Y_D, the flash-induced turnover of the S states is rapidly desynchronized as observed previously (*18*) due to misses, the presence of reduced Y_D, and the lack of a synchronizing preflash (*58*). A two-flash sample prepared with this reduction and flash protocol was dominated by the S_3 state, although it also contained a considerable fraction of centers in the S_2 state (*58*). The sample given three flashes was estimated to contain ∼50% PSII in the S_0 state and ∼40% in the S_3 state, which is normal in this type of samples.

EPR Spectroscopy. Low-temperature EPR measurements were performed in a completely dark laboratory with a Bruker ELEXYS500E spectrometer using a SuperX EPR049 microwave bridge and a Bruker ST4102 standard cavity. The system was fitted with an Oxford Instruments cryostat and temperature controller. The split EPR signals were induced by illumination directly in the cavity at 5 K via a light guide. The light intensity, measured at the position of the sample, was 40 or 160 W/m^2 using white light filtered through a 5 cm thick $CuSO_4$ (aqueous) filter. This illumination regime was applied for 20 s to induce the split signals if not otherwise indicated in the text.

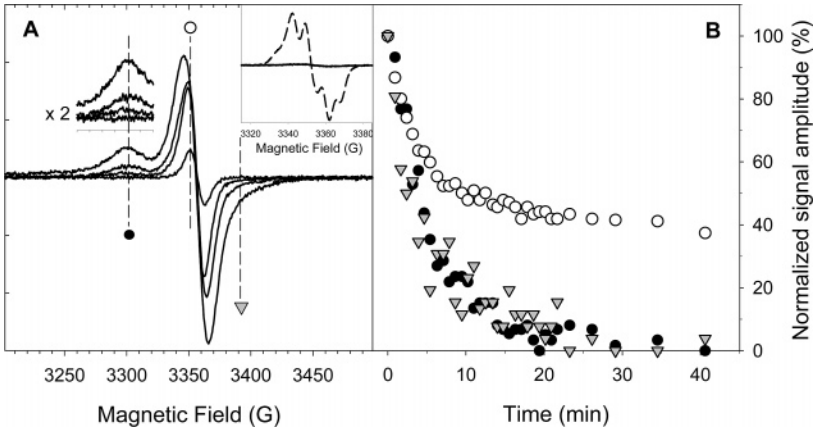

FIGURE 1: (A) Light minus dark difference spectrum of EPR signals induced by illumination at 5 K (10 s, 40 W/m^2) of a dark-adapted PSII sample dominated by the S_1 state. The spectra were recorded immediately after the illumination at different microwave powers (from top to bottom at 3300 G: 25 mW, 1.0 mW, 0.1 mW, and 1.0 μW). The low-field peak region is enlarged 2 times for clarity. The dashed lines with symbols indicate the field positions used in Figure 1B. The inset shows the EPR spectrum of $Y_D^\bullet$ before (dashed) and that remaining after the reduction treatment (black). (B) Decay in the dark at 5 K of the light-induced EPR spectrum recorded in the zero-flash sample at 25 mW, dominated by the "Split S_1" EPR signal. The decay is plotted at 3300 (●), 3350 (○), and 3390 G (gray triangles). The "Split S_1" peak at 3300 G showed a fast, single decay phase ($t_{1/2}$ = 3 min) involving the entire amplitude of the signal. The same decay kinetics were found for the shoulder at 3390 G (gray triangles). At the peak of the signal (3350 G), 54% of the amplitude decayed with similar kinetics and the rest decayed much slower. EPR parameters for panels A and B; temperature, 5 K; microwave frequency, 9.41 GHz; modulation amplitude, 4 G. EPR parameters for the inset: temperature, 15 K; microwave power, 1.0 μW; modulation amplitude, 3.2 G.

To determine the spectral shapes of the split signals, decay-associated EPR spectra were constructed. The split signal in each respective S state was induced by the defined illumination protocol, and an EPR spectrum was recorded immediately after illumination. The decay in the dark of the EPR signals was then followed by recording a new spectrum every minute for ~45 min. The change in the signal intensity at every field position was plotted versus time and analyzed. In our analysis of the "Split S_1" signal, a decay half-time of 3 min was found to encompass the total signal amplitude at the low-field peak at g = 2.035 (compare refs *46* and *48*). The amplitude of this decay phase at each field position was set to represent the decay kinetics that belonged to the split signal part of the light-induced spectrum. A plot of this amplitude at all field positions produced the decay-associated spectrum of the "Split S_1" signal. Similar protocols were applied to construct decay-associated spectra also for the signals originating from the S_0 state (in a three-flash sample) and the S_3 state (in a two-flash sample).

The microwave power needed to reach half-saturation, $P_{1/2}$, for the different signals was determined graphically from a plot of $\log(I/P^{0,5})$ versus $\log P$ (milliwatts) (*59*, *60*). I is the signal intensity at microwave power P. $P_{1/2}$ was found by extrapolating the linear parts of the curve to their intersecting point, where the $P_{1/2}$ value can be read on the abscissa directly.

Illumination of the sample for 3 min in room light (room temperature) followed by a 15 min dark adaptation provided complete oxidation of $Y_D^\bullet$ (*58*). The EPR signal from completely oxidized $Y_D^\bullet$ was used as an internal standard, and the signal was induced after all other measurements in each sample. At normal pH, $Y_D^\bullet$ is very stable, and after our pre-illumination and dark adaptation procedure, it is safe to assume that the reoxidized $Y_D^\bullet$ amounts to one radical per PSII center (fully oxidized $Y_D^\bullet$ equals one spin per PSII).

RESULTS

Spectral Resolution of the "Split S_1", "Split S_3", and "Split S_0" EPR Signals. The light-induced EPR signals from PSII at 5 K are complex spectra with components from the split signals and light-induced Car/Chl radicals. Normally, the $Y_D^\bullet$ radical EPR spectrum is very large and obscures the light-induced signals in the $g \sim 2.0$ region. To improve the spectral resolution of the light-induced EPR spectra, $Y_D^\bullet$ was chemically reduced before the different S states were induced by laser flashes. In those samples, the split signals were induced with weak light at 5 K. All light-induced EPR signals were observed overlaid on a small remaining $Y_D^\bullet$ (1.5%, Figure 1A, inset), but in the figures, illuminated minus dark difference spectra are shown, which eliminate the contribution from the small $Y_D^\bullet$.

Figure 1 describes the results for the "Split S_1" signal that was studied in the sample incubated in the dark (zero flashes). Figure 1A shows the difference spectra recorded at different microwave powers, immediately after the 10 s illumination. At an elevated microwave power (>1 mW), the EPR spectrum is dominated by the typical shoulder at 3300 G (marked with a filled circle) known to originate from the "Split S_1" signal and a large radical-like feature at $g \sim 2$. At a very low microwave power (1 μW), the shoulder at 3300 G is barely observable while the radical-like feature at $g \sim 2$ remains. The microwave power dependence of the EPR spectrum is further described below. Figure 1B shows the decay in the dark of the EPR signal amplitude at different field positions recorded at a microwave power of 25 mW. At 3300 G (●), the entire signal decayed with a single exponential ($t_{1/2}$ = 3 min; Table 1). This reflects the "Split S_1" decay, and the homogeneous decay kinetics indicates that the recorded spectrum is pure at this field position. The same monoexponential, complete decay was found on the shoulder at 3390 G (gray triangles), suggesting also a split signal component here. In contrast, at 3350 G (○), the fast

Table 1: Characteristics of the Light-Induced EPR Signals at 5 K

EPR signal	$t_{1/2}$ (min)[a]	$P_{1/2}$ (mW)
"Split S_1"	3	1
"Split S_3"	3 (40%)	5
"Split S_3"	slow[b] (60%)	
"Split S_0"	3	2
9 G wide radical[c]	>30	$\sim 5 \times 10^{-3}$

[a] $t_{1/2}$ for the decay in the dark at 5 K. [b] Fraction of slowly or nondecaying "Split S_3" signal. [c] Radical, probably from a Car/Chl species, that is oxidized by our illumination regime in an S-state-independent way.

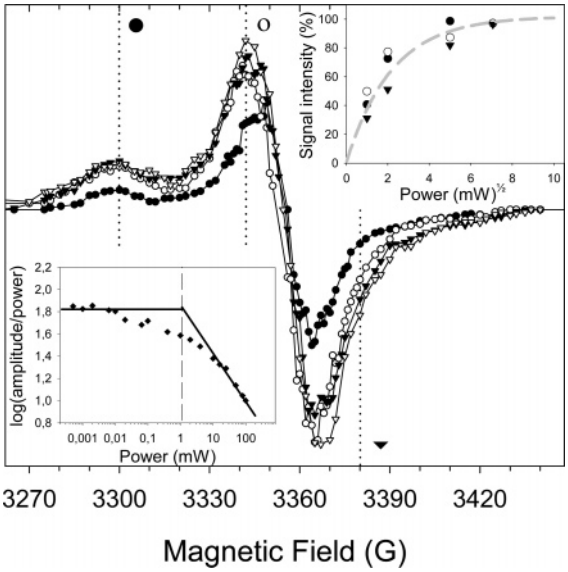

FIGURE 2: Decay-associated spectrum of the "Split S_1" EPR signal at different microwave powers. The amplitude of the fast-decaying part ($t_{1/2} = 3$ min) of the light-induced signal amplitude in the zero-flash sample, determined as described for Figure 1B, was used to construct the decay-associated spectrum of the "Split S_1" EPR signal. The spectra were obtained at 1 (●), 4 (○), 25 (▼), and 50 mW (▽). The inset in the bottom left corner shows the microwave power dependence of the amplitude at 3300 G (the "Split S_1" peak) plotted as log(amplitude/power$^{1/2}$) vs power (milliwatts, log scale). The data are from the spectra in Figure 1A and from spectra recorded at additional microwave powers. $P_{1/2}$ was determined to be 1 mW (*59*, *60*). In the inset in the top right corner, power saturation data from three different parts of the created spectrum [3330 (●), 3342 (○), and 3380 G (▼)] are plotted and compared to a simulated curve with a $P_{1/2}$ of 1 mW (gray dashed line). The dotted lines in the decay-associated spectrum indicate the field positions used to construct the inset. EPR parameters were as described for Figure 1.

decay ($t_{1/2} = 3$ min) encompassed only 54% of the total EPR signal, while the rest of the signal decayed very slowly. Thus, at 3350 G, the recorded spectrum is mixed and composed of one part from the split signal and one part from another species. This other species could be a Car or Chl radical (see below).

From this kinetic analysis, a decay-associated spectrum was created between 3260 and 3450 G (Figure 2) for the fast ($t_{1/2} \sim 3$ min) decaying signal. We propose that this spectrum reveals the "true" shape of the "Split S_1" signal: a peak centered at 3300 G, a shoulder around 3390 G, and a 20 G wide radical-like feature centered at 3355 G.

The remaining, slowly decaying part in the $g \sim 2.0$ region ($t_{1/2} > 30$ min) was a simple radical signal (Figure 3), 9.5 G wide and centered at 3357.5 G ($g = 2.0024 \pm 0.0001$). The

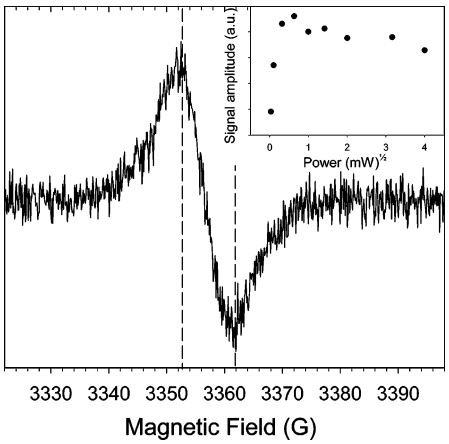

FIGURE 3: Induction of a stable radical ($t_{1/2} > 30$ min at 5 K) by a 20 s illumination (40 W/m^2) at 5 K in a zero-flash sample dominated by the S_1 state. The spectrum is recorded after a 43 min decay in the dark at 5 K of the light-induced signal. The line width (dashed lines) is 9.5 G, and the signal is centered at $g = 2.0024$. The inset shows the microwave power dependence of this radical EPR signal. The power for half-saturation ($P_{1/2}$) is ~ 5 μW. EPR parameters: temperature, 5 K; microwave frequency, 9.41 GHz; microwave power, 1 μW; modulation amplitude, 3.2 G.

radical was induced in ~5% of the PSII centers after illumination for 20 s at 40 W/m^2 as judged by double integration of the radical spectrum (compare also with the experiment described in Figure 4C; see below). When the light intensity is increased, more of this slowly decaying radical was formed, and a 20 s illumination at 160 W/m^2 gave rise to the radical in 10% of the PSII centers (not shown). The induction temperature (5 K), the width of this stable radical (9.5 G) (*13*), and the microwave power saturation at 5 K ($P_{1/2} \sim 5$ μW) (Figure 3, inset) indicated that this slowly decaying, light-induced species was a Car^+ radical, although an oxidized chlorophyll species cannot be ruled out.

The kinetic analysis of the illumination-induced species in the S_1 state (Figures 1 and 2) indicated that at least two spectral components were induced in the $g \sim 2.0$ region of the spectrum. We therefore analyzed this part of the spectrum in further detail. Panels A and B of Figure 4 show the decay-associated spectra, resolved in the $g \sim 2.0$ region, at microwave powers of 25 mW and 1 μW. Figure 4C shows the fraction of PSII involved in the fast-decaying (ca. 4% of PSII) and slow-decaying or nondecaying parts (ca. 5% of PSII) of the spectra. At a low microwave power (1.0 μW, Figure 4B,C), the spectrum representing the decaying part of the signal (●) was almost equal in size to the spectrum from the nondecaying part of the spectrum (○). At this low microwave power, both EPR spectra were recorded at or close to nonsaturating conditions, and the result indicates that approximately the same amount of spins was involved in each species. At a high microwave power (25 mW, Figure 4A), the amplitudes of the spectra were clearly different, and the decaying spectrum (●) was 2.7 times larger than the slow-decaying and nondecaying parts of the spectrum (○). Since both spectra represented approximately the same number of spins, the result indicates that the decaying part of the signal relaxes much faster than the nondecaying part of the spectrum. At a microwave power of 25 mW (Figure 4A), the nondecaying signal was severely saturated with

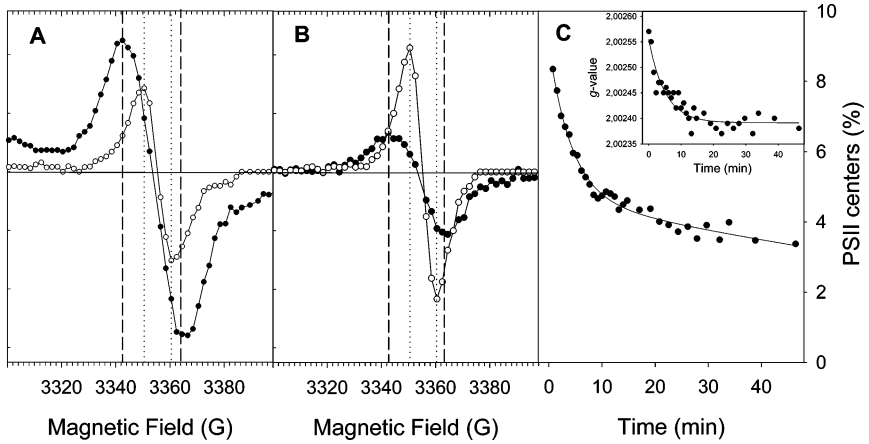

FIGURE 4: Decay-associated spectra in the $g \sim 2.0$ region recorded at (A) 25 mW and (B) 1.0 μW microwave powers after a 10 s illumination (40 W/m^2) at 5 K of a dark-adapted sample dominated by the S_1 state. The spectra represent the amplitude of the light-induced spectrum decaying with a $t_{1/2}$ of ~3 min (●) and the nondecaying fraction of the light-induced spectrum (○; compare Figure 3). The decaying spectrum had a line width of ca. 22 G (dashed lines), and the nondecaying spectrum had a line width of ca. 9.5 G (dotted lines). (C) Time-dependent decay of the radical feature measured on a PSII ($Y_D^\bullet$ total) basis during incubation in the dark after illumination at 5 K. The inset shows the time-dependent decrease in the g value of the spectral feature at $g \sim 2.0$ during the decay of the light-induced EPR signal. The spectra in panel C were recorded at a microwave power of 1.0 μW. EPR parameters: temperature, 5 K; microwave frequency, 9.41 GHz; modulation amplitude, 4 G.

microwaves (compare Figure 3, inset) while the decaying signal was only saturated to a minor extent (compare Figure 2, bottom inset), resulting in the relative amplitudes observed in Figure 4A.

We can thus conclude that the two spectral components represent totally different species that both are induced by the illumination at 5 K. This conclusion is further substantiated by the g values and line widths of the decay-associated spectra in Figure 4. The nondecaying part of the spectrum (○) was characterized by g values of 2.0026 and 2.0024 in the high- and low-power spectra, respectively, similar to the g value of, for example, Car and Chl radicals. In contrast, the decaying part of the spectrum (●) was characterized by g values of 2.0040 and 2.0033 in the high- and low-power decay-associated spectra, respectively. These g values are significantly higher than the g value of the Car and Chl radicals and closer to the g value of, for example, a tyrosine radical (*61*, *62*).

The difference between the g values found in the decay-associated spectra obtained at 25 mW and 1 μW [$t_{1/2} \sim 3$ min; Figure 4A,B (●)] can be attributed to the possible contribution from a fast-decaying Car radical[2] (*63*) that will be mixed in the g value under the nonsaturating conditions (1 μW, Figure 4B). In contrast at 25 mW, this Car_{fast} will be severely saturated and will consequently contribute less to the g value of the decaying part of the spectrum [Figure 4A (●)]. The slight difference in g value between the nondecaying spectra (○) at 25 mW and 1 μW most probably reflects the fact that the spectrum obtained at 25 mW is distorted by the high microwave power due to rapid passage effects.

During the decay of the light-induced spectrum, this resulted in a decrease in the apparent g value due to the progressively increasing domination of the nondecaying species (which exhibited a lower g value). This shift in the g value could be directly observed in the spectra recorded during the decay of the light-induced signal, and the time dependence of the g shift (recorded at a microwave power of 1 μW) is shown in the inset of Figure 4C. In the first spectrum, recorded after the 10 s illumination, the g value of the central feature was 2.0026. At this stage, the g value was a mix (ca. 50% of each, Figure 4C) of the g values for the decaying (radical involved in the split signal and possibly Car_{fast}) and nondecaying species (Car/Chl). The g value decreased with time in the dark to a stable g value of 2.0024 obtained after ca. 15 min. The half-time for this shift in the g value was ca. 3 min, indicating that it was directly correlated with the decay of the split part of the light-induced spectrum. The g shift could also be observed at higher microwave powers (not shown).

Interestingly, the decay-associated spectra in panels A and B of Figure 4 indicate that the line width of the spectral species decaying with a $t_{1/2}$ of ~3 min was ca. 22 G (dashed lines). The broad line width was observable at both high and low microwave powers. The decaying species was thus much wider than the nondecaying signal that was only ca. 9−10 G wide (dotted lines in panels A and B of Figure 4; compare also with Figure 3).

To obtain the unperturbed spectrum of the "Split S_3" signal, the decay kinetics of the light-induced signals at 5 K in a sample given two flashes were analyzed. The sample was dominated by the S_3 state but also contained a fraction of centers in the S_2 state due to misses in the turnover of the OEC. However, only the S_3 state will contribute to the light-induced split spectrum, since the S_2 state seemingly does not give rise to its own light-induced signals with our illumination protocol at 5 K. Figure 5A shows the light-induced minus dark difference spectra recorded at different microwave powers. The difference spectrum recorded at a microwave power of >1 mW was characterized by a broad peak at the low-field side of $g = 2$ and a trough with two peaks at high field. The spectrum also contained a radical-

[2] Optical spectroscopy experiments at 2 K in intact PSII revealed that light-induced Car^+ (induced by an illumination regime similar to that applied in our EPR experiments) decayed partly with a fast decay phase ($t_{1/2} \sim 5$ min) and partly with a slower decay phase ($t_{1/2} > 40$ min) (F. Ho, J. L. Hughes, K. G. V. Havelius, S. Styring, and E. Krausz, unpublished data).

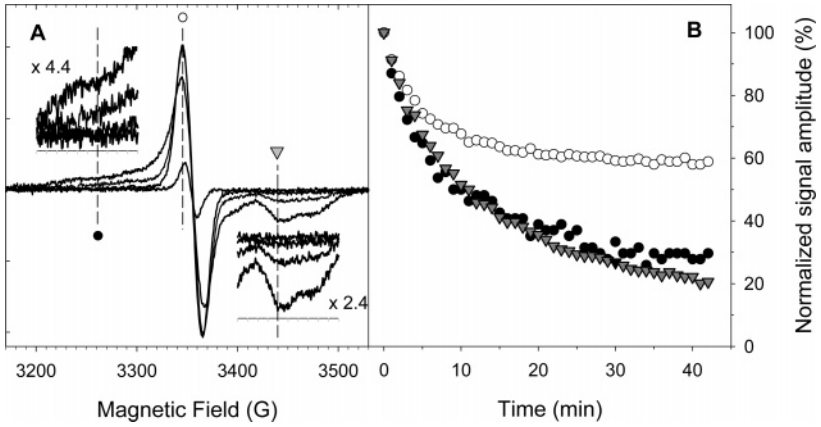

FIGURE 5: (A) Light minus dark difference spectra of EPR signals induced by illumination at 5 K (20 s, 40 W/m^2) of PSII samples subjected to two laser flashes and dominated by the S_3 state. The spectra were recorded immediately after the illumination at different microwave powers (from bottom to top at 3440 G: 32 mW, 1.0 mW, 0.1 mW, and 1.0 μW). The peak region around 3260 G and the trough region around 3440 G are enlarged for clarity. The dashed lines with symbols at 3260 (●), 3345 (○), and 3440 G (gray triangles) indicate the field positions where the decay traces in panel B were measured. (B) Decay in the dark at 5 K of the light-induced (20 s, 40 W/m^2) EPR spectrum recorded in the two-flash sample at a microwave power of 25 mW. In the decay traces at 3260 (●) and 3440 G (gray triangles), the fast-decaying phase with a $t_{1/2}$ of ~3 min encompassed 40 and 30% of the signal, respectively. A large part of the signal remained after 43 min. The trace measured at the middle peak [3345 G (○)] was dominated by the stable part (59%) but also contained a species decaying with a $t_{1/2}$ of ~3 min (32%). EPR parameters: temperature, 5 K; microwave frequency, 9.41 GHz; modulation amplitude, 10 G.

like feature centered at $g \sim 2.0$ quite similar to the "Split S_1" signal. In contrast, at a very low microwave power, the low- and high-field parts of the signal were hardly observable. Instead, the spectrum was dominated by a small radical feature around $g \sim 2.0$, which we also here interpret to belong mostly to an oxidized Car or Chl species. Figure 5B shows decay traces recorded at a high microwave power (25 mW) at 3260 (●), 3345 (○), and 3440 G (gray triangles), chosen to illustrate the decay kinetics of the light-induced signals over 43 min in the dark. At 3260 and 3440 G, the signal decayed with a $t_{1/2}$ of ~3 min (ca. 40 and 30%, respectively, of the total amplitude) and slower/nondecaying phases. It is clear from these decay traces that the signal did not decay to completion over our studied time interval (0−43 min). However, a complete decay, if possible to achieve, would involve EPR measurements over several hours, which are difficult to record with precision. Therefore, we were unable to determine the true decay half-time(s) for the slower phase. At 3345 G, ~30% of the signal decayed with a $t_{1/2}$ of ~3 min, while more than 60% of the signal was stable in the dark at 5 K in this time range. In this analysis, we have constructed decay-associated spectra for the fast-decaying part of the signal and the signal that remained in the spectrum after a 40 min decay period.

Figure 6A shows the decay-associated spectrum for the fast-decaying ($t_{1/2} \sim 3$ min) fraction of the spectrum in the two-flash sample. The fast-decaying "Split S_3" signal spectrum ($t_{1/2} \sim 3$ min) consisted of a broad peak centered at 3240 G, a slightly asymmetric derivative shape feature at 3354 G, and two troughs at 3440 and 3470 G. The nondecaying spectrum (Figure 6B, amplitude remaining after 43 min) was dominated by the shape of the Car or Chl radical species. Some "split-shaped" features were still observed at both wings in the spectrum, reflecting the fraction of the split spectrum that did not decay during 43 min.

A similar analysis was performed for the "Split S_0" EPR signal recorded at different microwave powers (Figure 7A). This was studied in a sample given three flashes that was dominated by the S_0 state. Due to misses, the sample also

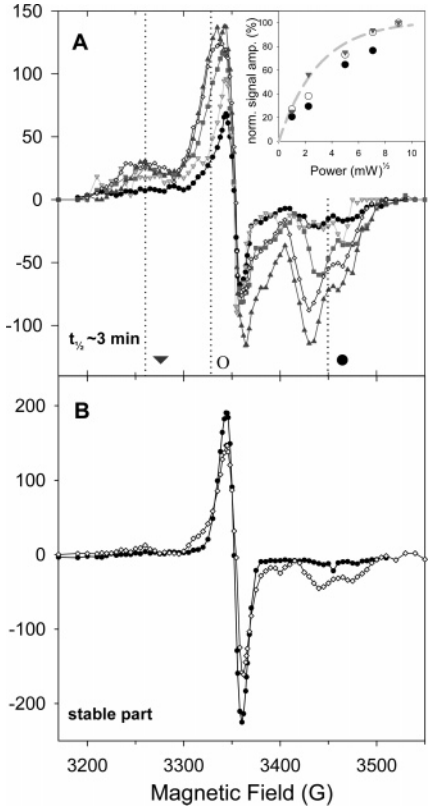

FIGURE 6: Decay-associated spectra of the "Split S_3" EPR signal. (A) The amplitude of the fast-decaying part ($t_{1/2} \sim 3$ min) of the light-induced signal amplitude in the two-flash sample, determined as described in the legend of Figure 5B, was used to construct the decay-associated spectrum of the "Split S_3" signal. The spectra were recorded at microwave powers of 1 (●), 5 (light gray triangles), 25 (gray squares), 50 (◇), and 81 mW (dark gray triangles). In the inset, power saturation data from three different parts of the created spectrum [3260 (gray triangles), 3335 (○), and 3450 G (●)] are plotted and compared to a simulated curve with a $P_{1/2}$ of 5 mW (gray dashed line). The dotted lines with symbols in the figure indicate the fields used in the inset. (B) Spectrum of the stable part of the signal remaining after a 43 min decay in the dark at 5 K in the two-flash sample created at microwave powers of 1 (●) and 50 mW (◇). EPR conditions were as described for Figure 5.

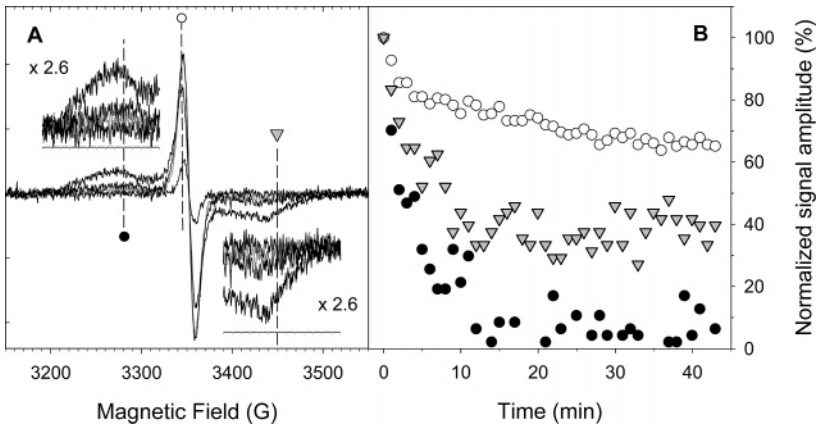

FIGURE 7: (A) Light minus dark difference spectra of EPR signals induced by illumination at 5 K (20 s, 40 W/m^2) of PSII samples subjected to three laser flashes and dominated by the S_0 state. The spectra were recorded immediately after the illumination at different microwave powers (from top to bottom at 3280 G: 25 mW, 1.0 mW, 0.2 mW, and 1.0 μW). The dashed lines with symbols indicate the field positions where the decay traces in panel B were measured. (B) Decay in the dark at 5 K of the light-induced (20 s, 40 W/m^2) EPR spectrum recorded in a three-flash sample. The decay traces were measured at 3280 (●), 3345 (○), and 3450 G (gray triangles). The peak at 3280 G (●) exhibited a fast single decay phase ($t_{1/2} = 3$ min) involving the entire amplitude of the signal. At the trough at 3450 G (gray triangles), 62% of the signal amplitude decayed with these kinetics, while the rest remained stable over the measurement (43 min). At the middle peak, 3345 G (○), 18% of the signal amplitude decayed fast ($t_{1/2} = 3$ min) and the rest much more slowly ($t_{1/2} > 30$ min). EPR conditions were as described for Figure 5.

contained a significant fraction of centers in the S_2 and S_3 states. At microwave powers of >1 mW, the low-field peak at 3280 G and a high-field trough at 3450 G dominated the spectrum together with the radical-like feature centered around $g \sim 2.0$. This spectrum is essentially similar to published EPR spectra of the "Split S_0" signal (*46*, *48*). At a low microwave power (1 μW), the low- and high-field features were almost absent from the spectrum, which only showed the radical (most probably dominated by the Car and/or Chl radical) in the middle part of the spectrum. In essence, this behavior is similar to that for the "Split S_1" and "Split S_3" signals. Figure 7B shows the decay of the light-induced spectrum measured at different field positions. At the low-field peak, 3280 G (●), 100% of the light-induced signal decayed with a $t_{1/2}$ of 3 min (Table 1), indicating that the spectrum was homogeneous at this field and that the entire "Split S_0" signal decayed in this time range. At 3450 G (gray triangles), 62% of the signal was decaying with fast kinetics ($t_{1/2} = 3$ min). The remaining 38% of the signal amplitude was not decaying in this time window (0−43 min), and we conclude that this fraction did not belong to the "Split S_0" signal. In the middle part of the signal [3340 G (○)], only 18% of the light-induced signal decayed fast, while the rest was slowly decaying ($t_{1/2} > 30$ min).

The slowly/nondecaying part of the signal at 3450 G (triangles, Figure 7B) reflected that a fraction of PSII in the three-flash sample was in the S_3 state. The "Split S_3" signal (Figures 5A and 6A) has a trough overlapping with the "Split S_0" signal at this field position. As described above, the overlapping "Split S_3" signal decayed both with fast ($t_{1/2} \sim$ 3 min) and slower/nondecaying decay kinetics (Figure 5B). The slowly decaying species will not interfere with the decay-associated spectrum of the "Split S_0" signal. However, the fast decay phase of the "Split S_3" EPR signal will be included in the total fast decay kinetics that builds up the decay-associated spectrum of the three-flash sample. The middle feature that decayed fast (18%) belonged mainly to the S_0-state signal and to some extent to the fast-decaying part of the S_3-state signal. However, only a minority of the PSII centers was in the S_3 state in the three-flash sample, and therefore, their contribution was quite small in the decaying part of the signal which was dominated by the "Split S_0" signal.

Figure 8 shows the spectrum associated with the $t_{1/2} = 3$ min decay phase in the sample given three flashes. The signal is composed of a 140 G wide symmetric split signal (centered at 3355 G) and a 20 G wide radical-like feature around 3355 G. The latter is very similar to what was found for the signal in the S_1 state, while the 140 G wide symmetric part is similar to what was described earlier for the "Split S_0" signal (Figure 7A) (*46*).

Microwave Power Saturation of the Split Signals. Field-swept spectra recorded at different microwave powers (Figure 1A, "Split S_1"; Figure 5A, "Split S_3"; Figure 7A, "Split S_0") allowed determination of the microwave power for half-saturation, $P_{1/2}$, for the different signals. For the "Split S_1" signal, the change in amplitude of the characteristic peak at 3300 G ($g = 2.035$) in a zero-flash sample was measured over a wide range of microwave powers, from 0.5 μW to 100 mW (Figure 2, bottom inset). The microwave power for half-saturation, $P_{1/2}$, for the "Split S_1" signal was 1 mW (Table 1). The microwave power saturation of the "Split S_0" EPR signal was monitored by the amplitude at the low-field peak, 3280 G, in a three-flash sample where the "Split S_3" signal did not interfere. The $P_{1/2}$ was 2 mW [Figure 8 , bottom inset (◆); Table 1]. The microwave power saturation of the "Split S_3" signal was measured at the trough at 3445 G in a two-flash sample [Figure 8, bottom inset (◇)]. The microwave power needed to saturate the "Split S_3" signal was even higher, and $P_{1/2}$ was 5 mW (Table 1). Thus, an unusually high microwave power was needed to saturate all three split signals compared to $P_{1/2}$ values in the microwatt range for most organic radicals, including the Car/Chl species studied in these experiments (Figures 3 and 4). This indicates that very fast relaxing species give rise to the split signals. This implicates the involvement of a transition metal in all signals, indicating that the $CaMn_4$ cluster is part of the split signals (*45*, *46*).

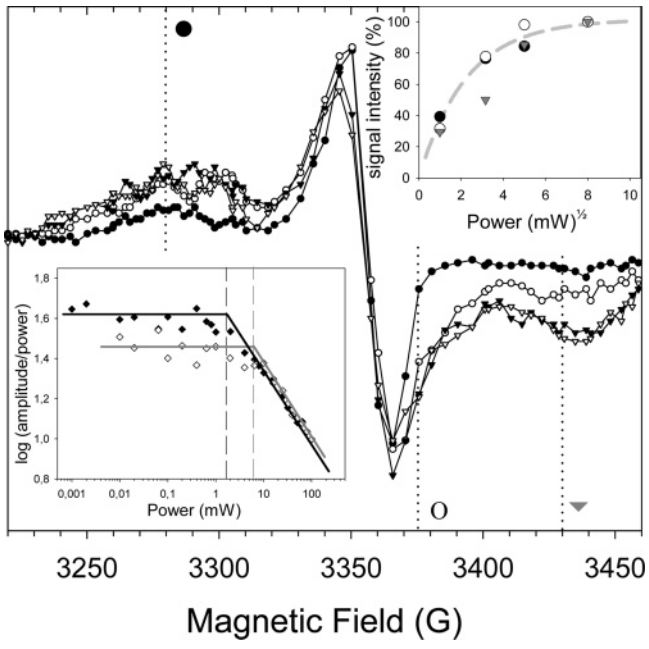

FIGURE 8: Decay-associated spectrum of the "Split S_0" EPR signal. The amplitude of the fast-decaying part ($t_{1/2} = 3$ min) of the light-induced signal amplitude in the three-flash sample, determined as described in the legend of Figure 7B, was used to construct the decay-associated spectrum of the "Split S_0" signal at several microwave powers. The spectra were obtained at microwave powers of 1 (●), 10 (○), 25 (▼), and 64 mW (▽). The inset in the bottom left corner shows the microwave power dependence at 3280 G (◆) in a three-flash sample (the "Split S_0" peak) and at 3445 G (◇) in a two-flash sample (the "Split S_3" trough). $P_{1/2}$ was determined to be 2 and 5 mW for the "Split S_0" and "Split S_3" signals, respectively. In the inset in the top right corner, power saturation data from three different parts of the created spectrum [3280 (●), 3375 (○), and 3430 G (gray triangles)] are plotted and compared to a simulated curve with a $P_{1/2}$ of 2 mW (gray dashed line). The dotted lines in the spectrum indicate the fields used in the inset. EPR conditions: temperature, 5 K; microwave frequency, 9.44 GHz; modulation amplitude, 10 G.

Microwave Power Saturation of the Decay-Associated Spectra. Decay-associated spectra of the "Split S_1" signal were created at several different microwave powers (Figure 2). The entire spectrum, illustrated by the field positions at 3300 (●), 3342 (○), and 3380 G (gray triangles) in Figure 2 (top inset), showed a microwave power dependence similar to that of the $P_{1/2}$ of the characteristic peak at 3300 G (Figure 2, top inset). This suggests that all parts of the signal originate from the same species.

The decay-associated spectrum of the "Split S_0" signal (see above) was constructed for several microwave powers. Figure 8 shows the spectra obtained at 1, 10, 25, and 64 mW. This allowed us to follow the relaxation of all parts of the signal in the decay-associated spectrum. This is illustrated at three field positions: 3280 (●), 3375 (○), and 3430 G (gray triangles) (Figure 8, top inset). The low-field side of the spectrum [Figure 8, top inset, 3280 G (●)] relaxed coherently with a $P_{1/2}$ of 2 mW [Figure 8, bottom inset (◆) and top inset (gray dashed line)]. The high-field trough [Figure 8, top inset, 3430 G (gray triangles)] was somewhat more difficult to saturate with microwaves. However, the high-field trough is a mix of the S_0- and S_3-state split signals. Therefore, the faster relaxation of the "Split S_3" signal [$P_{1/2} = 5$ mW; Figure 8, bottom inset (◇)] interferes significantly in the analysis and explains the difference in magnetic relaxation between the high-field and low-field sides in the decay-associated spectrum. Importantly, a part of the high-field side of the signal was not significantly mixed with the "Split S_3" signal, and it relaxed with a $P_{1/2}$ of 2 mW [Figure 8, top inset, 3375 G (○)]. To conclude, the relaxation of the >3400 G signal was closer to the $P_{1/2}$ of the "Split S_3" signal than the rest of the decay-associated spectrum of the three-flash sample, which relaxed with a $P_{1/2}$ of 2 mW.

Decay-associated spectra of the "Split S_3" signals (Figure 6) were created for several microwave powers: 1, 5, 25, 50, and 81 mW. The decay-associated spectrum based on the decay half-time ($t_{1/2}$) of ~3 min showed a similar relaxation pattern over the entire spectrum. This is illustrated in the inset of Figure 6A, where the signal amplitudes at three field positions [3260 (gray triangles), 3335 (○), and 3450 G (●)] were plotted versus the square root of the microwave power. The change in amplitude with microwave power was compared to the power saturation for the "Split S_3" signal (gray dashed line) obtained in a separate experiment of the total light-induced amplitude at 3445 G (see above). We conclude from this comparison that all the features in the $t_{1/2} \sim 3$ min decay-associated spectrum of the "Split S_3" signal reflected the same very fast relaxing species. The stable part of the spectrum in the two-flash sample (Figure 6B) was dominated by the slowly relaxing Car/Chl radical ($P_{1/2} \sim 5$ μW; Figure 3, inset; Table 1), while the small split wings displayed the hallmark of the fast-relaxing species.

DISCUSSION

In this paper, we have constructed decay-associated spectra reflecting the split EPR signals induced by illumination at 5 K of PSII positioned in the S_1, S_3, and S_0 states. Their microwave power saturation characteristics were determined and found to be consistent over the entire spectrum but different between the three split signals.

The OEC-related split EPR signals have been studied since 1989, when the first papers were published of a split EPR signal from $S_2Y_Z^\bullet$ in Ca^{2+}-depleted PSII (*24*, *25*). In many of the previous publications, the middle part around $g \sim 2.0$ has been excluded from the spectrum because the $Y_D^\bullet$ radical dominates in this region. The consequence is that possible contributions to the split signal around $g \sim 2.0$ have been cut out and ignored. We have overcome this problem by chemical reduction of the $Y_D^\bullet$ before measurements. This opened a spectral window in the $g \sim 2$ region, since our illumination protocol did not oxidize Y_D at 5 K (at pH 6.3).[3] Another obstacle to overcome before we could describe the true shape of the split signals was the fact that our illumination protocol induced an organic radical together with the split signal (independent of the S state). However, the decay kinetics of the split signals and the organic radical in the dark were different. Thereby, the fast-decaying split signals could be separated from the slowly decaying organic radical by decay-associated spectral analysis.

[3] In Mn-depleted PSII, oxidation of Y_D at 15 K has been demonstrated, but this only occurs at high pH and is steered with a pK_a of ~7.6 for a single protonatable group (*64*).

The "Split S_1" EPR spectrum (Figure 2) ($t_{1/2} = 3$ min) was composed of one "split" part, which was ~80 G wide centered around 3342 G, and a more radical-like part, which was 22 G wide centered at 3355 G. These two parts could be separated neither by decay time nor by microwave power saturation, and we conclude that they together constitute the true experimental shape of the "Split S_1" signal spectrum. The "Split S_1" signal spectrum has been simulated at two microwave frequencies, X- and W-band (*47*). At X-band, the overall features in the simulated spectrum were similar to those of our experimental spectrum, including both the low-field peak and the central radical-like signal (Figure 2), which strengthens the validity of the simulation. In the theoretical analysis, the system involved magnetic interaction between the organic radical and both the ground and first excited spin states of the $CaMn_4$ cluster in the S_1 state ($S = 0$ and $S = 1$, respectively). The "Split S_1" signal originates from spin multiplet M2, which arises from the exchange coupling between the first excited $S = 1$ state of the Mn cluster and the $S = {}^1/_2$ state of the interacting radical, presumably $Y_Z^\bullet$. Thus, the "Split S_1" signal has been linked to the first excited, $S = 1$, spin state of the $CaMn_4$ cluster (*47*). However, the theoretical model (*47*) does not exclude population also of the M1 ground state ($S = {}^1/_2$) of the involved radical at a very low temperature. Therefore, the EPR spectrum might also contain a contribution from the radical species itself even if this might not be easily observed in the presence of the interaction signal.

In the absence of direct experimental proof, the radical involved in these light-induced split signals is thought to be $Y_Z^\bullet$. A strong argument for this assignment is the suitable, short distance (ca. 6 Å) between Y_Z and the $CaMn_4$ cluster, which is necessary to explain this kind of split EPR signal (*2*−*6*, *11*), the spectral similarities with other split signals from the $S_2Y_Z^\bullet$ state in inhibited PSII centers, and the ability to form a ML signal at 77 K from the split-containing samples under certain conditions (*45*).

The data here might provide further evidence for the assignment of $Y_Z^\bullet$ as the radical that is involved in the "Split S_1" signal. Detailed investigation of the radical feature in the "Split S_1" signal (Figure 4) showed that the signal was characterized by a relatively high g value (2.0033−2.0040) and a broad line width (22 G). $P_{1/2}$ was determined to be ~1 mW at 5 K (Figure 2), which is unusually high for a free radical. Among the known radical species in PSII, $Y_D^\bullet$ in PSII centers in the S_1 state has a $P_{1/2}$ of ~46 μW at 8 K (*60*), while the Car/Chl radical studied here has a $P_{1/2}$ of ~5 μW (Table 1). In contrast, $Y_Z^\bullet$ relaxes much faster due to cross relaxation with the close-lying $CaMn_4$ cluster. There are no relaxation measurements available for $Y_Z^\bullet$ at 5 K in the presence of a fully active $CaMn_4$ cluster. However, in Ca^{2+}-depleted PSII centers, $Y_Z^\bullet$ was found to have a $P_{1/2}$ of >50 mW while $Y_D^\bullet$ was a slower relaxer with a $P_{1/2}$ of 8−10 mW at room temperature (*41*). Thus, the fast relaxation of the radical points to the involvement of $Y_Z^\bullet$. An analogous argument can be made for the line width. The signal was 22 G wide (the line width at half-height). This is very different from those of Car and Chl radicals, which are 9−11 G wide (*65*; compare Figure 3), while $Y_Z^\bullet$ has a line width of 19−22 G (*22*, *65*). Thus, the broad line width also suggests the direct involvement of a tyrosine radical, presumably $Y_Z^\bullet$ (due to the fast relaxation; see above), in the light-induced spectrum.

The assignment of the radical spectrum to $Y_Z^\bullet$ is further supported by the g value (2.0033−2.0040, Figure 4A,B) that was significantly higher than that for a Car radical (2.0024; *13*) and closer to that of $Y_Z^\bullet$ (2.0046; *22*, *61*, *65*). However, the g value we obtained (2.0033−2.0040) is smaller than that normally reported for $Y_Z^\bullet$ (2.0046). In this respect, it is interesting that the g value of a tyrosine radical is very dependent on the protonation state of the radical with g values ranging from 2.0032 for fully protonated tyrosine radicals (*66*) to the higher g values reported for the deprotonated tyrosine radicals in, for example, PSII (2.0046), ribonucleotide reductase (2.0050) (*62*, *67*), and a synthetic Ru-Tyr molecule (2.0045) (*68*). The lower g value we observe could thus be interpreted to indicate that $Y_Z^\bullet$ is partially protonated when formed in intact PSII by illumination at a very low temperature (5 K).

Formation of a protonated tyrosine radical has precedence in the literature, and a g value of 2.0029 was found in a Ru-Tyr-dpa compound (*69*), where the phenolic proton was locked in a hydrogen bond. A very similar situation was also reported for the light-induced oxidation of $Y_D^\bullet$ in Mn-depleted PSII at elevated pH (*70*). In this case, illumination at 1.8 K resulted in the formation of a partially protonated $Y_D^\bullet$ radical. This was recognized in high-field EPR by an unusually low g_x of 2.00643. Relaxation at 77 K resulted in a shift to 2.00756 typical for $Y_D^\bullet$ generated at physiological temperatures. This was interpreted to indicate that the $Y_D^\bullet$ radical induced at 1.8 K was involved in a hydrogen bond to the nearby D2-His190, but at the low temperature, the proton remained closer to Y_D than normal.

Our observation here of a relatively low g value also for the radical we assign to $Y_Z^\bullet$ indicates a similar situation also around Y_Z. It has been suggested (*46*) that Y_Z is involved in a low-barrier hydrogen bond. Here we extend this conclusion and suggest that deprotonation along this bond at 5 K results in a radical in which the phenolic proton resides abnormally close to the phenolic oxygen. This suggestion implies a restricted proton movement in the hydrogen bond and is also indicative that Y_Z is protonated prior to oxidation, at least in the S_1 state.

The observation of both a split signal and free $Y_Z^\bullet$ from the same redox state also has precedence in the literature. In Ca^{2+}-depleted PSII, the state that gives rise to the split $S_2Y_Z^\bullet$ magnetic interaction signal (always recorded at 5−15 K) has been suggested to contain a considerable fraction of free, magnetically uncoupled $Y_Z^\bullet$ when the EPR spectrum is recorded at room temperature (*30*, *36*, *39*, *41*). Albeit disputed (*71*, *72*), these results from many groups indicate that $Y_Z^\bullet$ can behave as a free form or as a form magnetically coupled to the same redox state of the $CaMn_4$ cluster. Such a situation would be consistent with $Y_Z^\bullet$ having the ability to populate either the M1 or the M2 state in the theoretical model for the "Split S_1" signal (*47*). Whether the population ratio follows a pure Bolzman distribution or if factors involving the molecular structure around $Y_Z^\bullet$ and the $CaMn_4$ cluster are involved cannot be decided at this stage.

The "Split S_0" EPR spectrum (Figures 7 and 8) ($t_{1/2} = 3$ min) was also composed of two "parts": the broad split part (140 G) and the narrow radical-like part (~20 G) both centered at 3355 G that could not be separated by either

decay time or microwave power saturation. Thus, the 20 G radical-like feature of the "Split S_0" signal behaves as a real part of the signal spectrum, videlicet, with the same decay kinetics and relaxation behavior as the broad split part. When the "Split S_0" signal was discovered, it was immediately observed that the symmetry of the broad part of the signal resembled that of the earlier studied $S_2Y_Z^\bullet$ split signals in inhibited PSII (*46*). There are several simulations of these signals (*35*, *37*, *38*, *40*), and the signal shape has been found to be very dependent on the nature of the magnetic coupling (exchange and dipolar) and the distance between the interacting spin systems. However, neither of the simulations has predicted the existence of a narrow radical-like feature in the center of the split signal in the inhibited systems. It is therefore highly relevant that such a narrow radical part was observed in the $S_2Y_Z^\bullet$ signal in acetate-treated PSII from a mutant lacking Y_D (D2-Y160F) (*54*). As in our case, the mutant allowed studies of the split signals without the spectral overlap of $Y_D^\bullet$. In this work, the narrow central line was described for the first time in addition to the expected splitting of the $S_2Y_Z^\bullet$ signal in acetate-treated PSII. The authors pointed out that new simulation attempts were probably needed to explain the unexpected middle part of the spectrum. Our new data, which define the central component together with the broad splitting as the "Split S_0" signal, strengthen the conclusion that new simulations of the split signals must also explain radical-like features in the spectra similar to what has been achieved for the "Split S_1" signal (*47*).

The decay-associated spectrum of the "Split S_3" signal based on a $t_{1/2}$ of ~3 min from spinach PSII (Figure 6A) was very similar in shape to the IR-induced S_3 signal recorded in a mutant from *T. elongatus* lacking Y_D (*54*). The different parts of the fast-decaying signal ($t_{1/2} \sim 3$ min) could not be separated by the microwave power saturation and behaved as one signal with a $P_{1/2}$ of ~5 mW (Figure 6A, inset). Both our spectrum and the spectrum from *T. elongatus* are characterized by a peak at 3260 G, two troughs at 3440 and 3470 G, and a narrow signal in the $g \sim 2$ region of the spectrum. The narrow signal in the $g \sim 2$ region had a somewhat broader peak and a smaller asymmetric trough around $g \sim 2$ (Figure 6A and ref *54*) compared to the radical-like features of the "Split S_1" and "Split S_0" signals. In the literature, the "Split S_3" signal is induced by NIR illumination at 50 K (*51*, *54*, *73*). Here we have used light filtered through a 5 cm thick $CuSO_4$ (aqueous) filter, which eliminates the IR light.[4] We induce the split signal at 5 K and measure it immediately, while in previous publications, the signal was induced at 50 K and then measured at 4 K. The time it takes to transfer the sample between 50 and 4 K is likely to involve the substantial decay of any decaying spectral parts and could give rise to a smaller signal size. This makes a straightforward comparison between the NIR-induced signal and our "Split S_3" signal difficult.

All three split signals are difficult to saturate with microwaves; consequently, they reflect species that relax very fast. This has been found before (*45*, *46*), but our analysis here demonstrates the same relaxation behavior for the entire spectra. This is particularly important for the narrow middle part which earlier has been difficult to study due to overlaying signals from different radical species ($Y_D^\bullet$, Car, and Chl_Z). However, these other radicals relax much slower than the split signals, which allowed studies of the latter at very high microwave powers. The fast relaxation behavior of the split signals indicates that very fast relaxers are involved in the signal and strongly implicates the involvement of the $CaMn_4$ cluster. This holds also for the $S_2Y_Z^\bullet$ split signal in inhibited PSII (as Ca^{2+} or Cl^- depleted) (*24*, *28*, *40*, *41*). It is interesting to note that the relaxation behavior is S-state-dependent. At 5 K, the "Split S_1" signal is easier to saturate than the "Split S_0" signal, which is easier to saturate than the "Split S_3" signal (Table 1). S-State-dependent relaxation enhancement of the $Y_D^\bullet$ radical has previously been observed (*60*, *74*). Due to cross relaxation between $Y_D^\bullet$ and the fast-relaxing $CaMn_4$ cluster, the microwave power saturation of $Y_D^\bullet$ in the presence of the different S states showed a clear difference between the S_1 state, with the lowest $P_{1/2}$ (46 μW at 8 K), and the other S states ($P_{1/2} > 105$ μW at 8 K). The relaxation enhancement was strongly temperature dependent, and the S_2 and S_3 states proved to have very similar relaxations. Since we have not detected any split signal from PSII in the S_2 state, a full comparison with the earlier data cannot be made, but it is clear that the "Split S_3" signals relaxed significantly faster than the "Split S_1" signal. It is thus likely that the S-state-dependent relaxation enhancement of the split signals and the $Y_D^\bullet$ radical has the same origin.

The slowly decaying radical we observed in low yield together with the split signals is presumably a carotenoid radical, but a chlorophyll radical cannot be excluded. The resolution in our spectrum might not be sufficiently good for the assignment of the radical to either Car or Chl. However, earlier studies on the light-induced radicals in intact PSII have revealed that a Car is the preferred donor at a very low induction temperature (20 K) (*75*). In Mn-depleted PSII, some studies observe only Car^+ formation upon illumination at 20 K (*13*), while many others find that illumination at ≥6 K oxidized both Car and Chl (*14*, *63*). The different P_{680}^+ electron donors available in our reduced samples at 5 K were Car/Chl, Cyt b_{559}, and the split donor. The Car^+/Chl^+ and Cyt b_{559}^{ox} formed by the illumination could be quantified. Our short and weak illumination at 5 K (40 W/m^2, 20 s) resulted in oxidation of Cyt b_{559} in ~8% of the PSII centers (not shown) and in the oxidation of ca. 5% Car/Chl. An increased level of illumination resulted in further oxidation of both species in addition to the formation of larger split signals. The maximum induction level of the "Split S_1" signal (not shown) in this study was quite similar to that in refs *46* and *48*. Zhang et al. (*48*) found 11% oxidation of Cyt b_{559} and oxidation of 16% Car/Chl under their particular experimental conditions. By also following the acceptor side, they could assign ~40% of the PSII to form the split signal in the S_1 state. In our PSII preparation from higher plants, we have not been able to investigate the acceptor side quantitatively due to the presence of the exogenous acceptor P*p*BQ, but it seems reasonable to assume the same order of magnitude as published earlier (*48*).

[4] We have observed that the "Split S_3" signal can be induced using monochromatic light at 532 nm (J.-H. Su, K. G. V. Havelius, F. Ho, F. Mamedov, and S. Styring, manuscript in preparation).

CONCLUSION

The three split EPR signals that were investigated, "Split S_1", "Split S_3", and "Split S_0", all exhibit spectral features in the $g \sim 2$ region together with, for each signal, characteristic peaks and troughs. It would be very improbable that the wings and the middle part of the split spectra be derived from different signals, since their decay kinetics and relaxation behavior are identical. Therefore, these spectra can provide the basis for further simulation studies of the split signals in higher plants. In addition, it is highly likely that the EPR spectrum, at least in the S_1 state, also contains a contribution from $Y_Z^\bullet$, spectroscopically distinguishable as a fast-relaxing radical spectrum resolved in the decay-associated spectrum. A small amount of Car/Chl was also oxidized in all cases, but this radical had clearly distinguishable relaxation and decay characteristics.

ACKNOWLEDGMENT

We thank Dr. Felix Ho for valuable discussions and sharing of data during the preparation of the manuscript and Dr. Ron Pace for helpful discussion of data.

REFERENCES

1. Barber, J. (2003) Photosystem II: The engine of life, *Q. Rev. Biophys. 36*, 71−89.
2. Zouni, A., Witt, H.-T., Kern, J., Fromme, P., Krauss, N., Saenger, W., and Orth, P. (2001) Crystal structure of photosystem II from *Synechococcus elongatus* at 3.8 Å resolution, *Nature 409*, 739−743.
3. Kamiya, N., and Shen, J.-R. (2003) Crystal structure of oxygen-evolving photosystem II from *Thermosynechococcus vulcanus* at 3.7-Å resolution, *Proc. Natl. Acad. Sci. U.S.A. 100*, 98−103.
4. Ferreira, K. N., Iverson, T. M., Maghlaoui, K., Barber, J., and Iwata, S. (2004) Architecture of photosynthetic oxygen-evolving center, *Science 303*, 1831−1838.
5. Kern, J., Loll, B., Zouni, A., Saenger, W., Irrgang, K.-D., and Biesiadka, J. (2005) Cyanobacterial photosystem II at 3.2 Å resolution: The plastoquinone binding pockets, *Photosynth. Res. 84*, 153−159.
6. Loll, B., Kern, J., Saenger, W., Zouni, A., and Biesiadka, J. (2005) Towards complete cofactor arrangement in the 3.0 Å resolution structure of photosystem II, *Nature 438*, 1040−1044.
7. Rappaport, F., and Lavergne, J. (1997) Charge recombination and proton transfer in manganese-depleted photosystem II, *Biochemistry 36*, 15294−15302.
8. Mamedov, F., Sayre, R. T., and Styring, S. (1998) Involvement of Histidine 190 on the D1 protein in electron/proton-transfer reactions on the donor side of photosystem II, *Biochemistry 37*, 14245−14256.
9. Hays, A.-M. A., Vassiliev, I. R., Golbeck, J. H., and Debus, R. J. (1998) Role of D1-His190 in proton-coupled electron transfer reactions in photosystem II: A chemical complementation study, *Biochemistry 37*, 11352−11365.
10. Berthomieu, C., Hienerwadel, R., Boussac, A., Breton, J., and Diner, B. A. (1998) Hydrogen bonding of redox-active tyrosine Z of photosystem II probed by FTIR difference spectroscopy, *Biochemistry 37*, 10547−10554.
11. Biesiadka, J., Loll, B., Kern, J., Irrgang, K.-D., and Zouni, A. (2004) Crystal structure of cyanobacterial photosystem II at 3.2 Å resolution: A closer look at the Mn-cluster, *Phys. Chem. Chem. Phys. 6*, 4733−4736.
12. Kok, B., Forbush, B., and McGloin, M. (1970) Cooperation of charges in photosynthetic O_2 evolution. I. A linear four-step mechanism, *Photochem. Photobiol. 11*, 467−475.
13. Hanley, J., Deligiannakis, Y., Pascal, A., Faller, P., and Rutherford, A. W. (1999) Carotenoid oxidation in photosystem II, *Biochemistry 38*, 8189−8195.
14. Tracewell, C. A., Cua, A., Stewart, D. H., Bocian, D. F., and Brudvig, G. W. (2001) Characterization of carotenoid and chlorophyll photooxidation in photosystem II, *Biochemistry 40*, 193−203.
15. Mamedov, F., and Styring, S. (2003) Logistics in the life cycle of photosystem II: Lateral movement in the thylakoid membrane and activation of electron transfer, *Physiol. Plant. 119*, 328−336.
16. Frank, H., and Brudvig, G. W. (2004) Redox function of carotenoids in photosynthesis, *Biochemistry 43*, 8607−8615.
17. Magnuson, A., Rova, M., Mamedov, F., Fredriksson, P.-O., and Styring, S. (1999) The role of cytochrome b_{559} and tyrosine$_D$ in protection against photoinhibition during in vivo photoactivation of photosystem II, *Biochim. Biophys. Acta 1411*, 180−191.
18. Styring, S., and Rutherford, A. W. (1987) In the oxygen-evolving complex of photosystem II the S_0 state is oxidized to the S_1 state by D^+ (signal II_{slow}), *Biochemistry 26*, 2401−2405.
19. Vass, I., and Styring, S. (1991) pH-dependent charge equilibria between tyrosine-D and the S states in photosystem II. Estimation of relative midpoint redox potentials, *Biochemistry 30*, 830−839.
20. Commoner, B., Heise, J. J., and Townsend, J. (1956) Light-induced paramagnetism in chloroplasts, *Proc. Natl. Acad. Sci. U.S.A. 42*, 710−718.
21. Babcock, G. T., and Sauer, K. (1975) A rapid, light-induced transient in electron paramagnetic resonance signal II activated upon inhibition of photosynthetic oxygen evolution, *Biochim. Biophys. Acta 376*, 315−328.
22. Hoganson, C. W., and Babcock, G. T. (1988) Electron-transfer events near the reaction center in O_2-evolving photosystem II preparations, *Biochemistry 27*, 5848−5855.
23. Debus, R. J. (1992) The manganese and calcium ions of photosynthetic oxygen evolution, *Biochim. Biophys. Acta 1102*, 269−352.
24. Boussac, A., Zimmermann, J.-L., and Rutherford, A. W. (1989) EPR signals from modified charge accumulation states of the oxygen evolving enzyme in Ca^{2+}-deficient photosystem II, *Biochemistry 28*, 8984−8989.
25. Sivaraja, M., Tso, J., and Dismukes, G. C. (1989) A calcium-specific site influences the structure and activity of the manganese cluster responsible for photosynthetic water oxidation, *Biochemistry 28*, 9459−9464.
26. Boussac, A., Zimmermann, J.-L., Rutherford, A. W., and Lavergne, J. (1990) Histidine oxidation in the oxygen-evolving photosystem-II enzyme, *Nature 347*, 303−306.
27. Ono, T., and Inoue, Y. (1990) Abnormal redox reactions in photosynthetic O_2-evolving centers in NaCl/EDTA-washed PS II. A dark-stable EPR multiline signal and an unknown positive charge accumulator, *Biochim. Biophys. Acta 1020*, 269−277.
28. Baumgarten, M., Philo, J. S., and Dismukes, G. C. (1990) Mechanism of photoinhibition of photosynthetic water oxidation by Cl^- depletion and F^- substitution: Oxidation of a protein residue, *Biochemistry 29*, 10814−10822.
29. Andréasson, L.-E., and Lindberg, K. (1992) The inhibition of photosynthetic oxygen evolution by ammonia probed by EPR, *Biochim. Biophys. Acta 1100*, 177−183.
30. Hallahan, B. J., Nugent, J. H. A., Warden, J. T., and Evans, M. C. W. (1992) Investigation of the origin of the "S3" EPR signal from the oxygen-evolving complex of photosystem 2: The role of tyrosine Z, *Biochemistry 31*, 4562−4573.
31. MacLachlan, D. J., and Nugent, J. H. A. (1993) Investigation of the S3 electron paramagnetic resonance signal from the oxygen-evolving complex of photosystem II: Effect of inhibition of oxygen evolution by acetate, *Biochemistry 32*, 9772−9780.
32. van Vliet, P., Boussac, A., and Rutherford, A. W. (1994) Chloride-depletion effects in the calcium-deficient oxygen-evolving complex of photosystem II, *Biochemistry 33*, 12998−13004.
33. van Vliet, P., and Rutherford, A. W. (1996) Properties of the chloride-depleted oxygen-evolving complex of photosystem II studied by electron paramagnetic resonance, *Biochemistry 35*, 1829−1839.
34. Szalai, V. A., and Brudvig, G. W. (1996) Formation and decay of the S3 EPR signal species in acetate-inhibited photosystem II, *Biochemistry 35*, 1946−1953.
35. Force, D. A., Randall, D. W., and Britt, R. D. (1997) Proximity of acetate, manganese, and exchangeable deuterons to tyrosine $Y_Z^\bullet$ in acetate-inhibited photosystem II membranes: Implications for the direct involvement of $Y_Z^\bullet$ in water-splitting, *Biochemistry 36*, 12062−12070.
36. Lydakis-Simantiris, N., Dorlet, P., Ghanotakis, D. F., and Babcock, G. T. (1998) Kinetic and spectroscopic properties of the $Y_Z^\bullet$ radical in Ca^{2+}- and Cl^--depleted photosystem II preparations, *Biochemistry 37*, 6427−6435.
37. Dorlet, P., Di Valentin, M., Babcock, G. T., and McCracken, J. L. (1998) Interaction of $Y_Z^\bullet$ with its environment in acetate-treated

photosystem II membranes and reaction center cores, *J. Phys. Chem. B 102*, 8239−8247.
38. Lakshmi, K. V., Eaton, S. S., Eaton, G. R., Frank, H. A., and Brudvig, G. W. (1998) Analysis of dipolar and exchange interaction between manganese and tyrosine Z in the $S_2Y_Z^\bullet$ state of acetate-inhibited photosystem II via EPR spectral simulations at X- and Q-bands, *J. Phys. Chem. B 102*, 8327−8335.
39. Szalai, V. A., Kühne, H., Lakshmi, K. V., and Brudvig, G. W. (1998) Characterization of the interaction between manganese and tyrosine Z in acetate-inhibited photosystem II, *Biochemistry 37*, 13594−13603.
40. Dorlet, P., Boussac, A., Rutherford, A. W., and Un, S. (1999) Multifrequency high-field EPR study of the interaction between the tyrosyl Z radical and the manganese cluster in plant photosystem II, *J. Phys. Chem. B 103*, 10945−10954.
41. Andréasson, L.-E., Vass, I., and Styring, S. (1995) Ca^{2+} depletion modifies the electron transfer on the both donor and acceptor sides in photosystem II from spinach, *Biochim. Biophys. Acta 1230*, 155−164.
42. Gilchrist, M. L., Ball, J. J. A., Randall, D. W., and Britt, R. D. (1995) Proximity of the manganese cluster of photosystem II to the redox-active tyrosine Y_Z, *Proc. Natl. Acad. Sci. U.S.A. 92*, 9545−9549.
43. Tang, X.-S., Randall, D. W., Force, D. A., Diner, B. A., and Britt, R. D. (1996) Manganese-tyrosine interaction in the photosystem II oxygen-evolving complex, *J. Am. Chem. Soc. 118*, 7638−7639.
44. Astashkin, A. V., Mino, H., Kawamori, A., and Ono, T. (1997) Pulsed EPR study of the S_3' signal in the Ca^{2+}-depleted photosystem II, *Chem. Phys. Lett. 272*, 506−516.
45. Nugent, J. H. A., Muhiuddin, I. P., and Evans, M. C. W. (2002) Electron transfer from the water oxidizing complex at cryogenic temperatures: The S_1 to S_2 step, *Biochemistry 41*, 4117−4126.
46. Zhang, C., and Styring, S. (2003) Formation of split electron paramagnetic resonance signals in photosystem II suggests that $tyrosine_Z$ can be photooxidized at 5 K in the S_0 and S_1 states of the oxygen-evolving complex, *Biochemistry 42*, 8066−8076.
47. Koulougliotis, D., Teutloff, C., Sanakis, Y., Lubitz, W., and Petrouleas, V. (2004) The $S_1Y_Z^\bullet$ metalloradical intermediate in photosystem II: An X- and W-band EPR study, *Phys. Chem. Chem. Phys. 6*, 4859−4863.
48. Zhang, C., Boussac, A., and Rutherford, A. W. (2004) Low-temperature electron transfer in photosystem II: A tyrosyl radical and a semiquinone charge pair, *Biochemistry 43*, 13787−13795.
49. Petrouleas, V., Koulougliotis, D., and Ioannidis, N. (2005) Trapping of metalloradical intermediates of the S-states at liquid helium temperatures. Overview of the phenomenology and mechanistic implications, *Biochemistry 44*, 6723−6728.
50. Koulougliotis, D., Shen, J.-R., Ioannidis, N., and Petrouleas, V. (2003) Near-IR irradiation of the S_2 state of the water oxidizing complex of photosystem II at liquid helium temperatures produces the metalloradical intermediate attributed to $S_1Y_Z^\bullet$, *Biochemistry 42*, 3045−3053.
51. Ioannidis, N., and Petrouleas, V. (2000) Electron paramagnetic resonance signals from the S_3 state of the oxygen-evolving complex. A broadened radical signal induced by low-temperature near-infrared light illumination, *Biochemistry 39*, 5246−5254.
52. Ioannidis, N., and Petrouleas, V. (2002) Decay products of the S_3 state of the oxygen-evolving complex of photosystem II at cryogenic temperatures. Pathways to the formation of the $S = 7/2$ S_2 state configuration, *Biochemistry 41*, 9580−9588.
53. Ioannidis, N., Nugent, J. H. A., and Petrouleas, V. (2002) Intermediates of the S_3 state of the oxygen-evolving complex of photosystem II, *Biochemistry 41*, 9589−9600.
54. Sugiura, M., Rappaport, F., Brettel, K., Noguchi, T., Rutherford, A. W., and Boussac, A. (2004) Site-directed mutagenesis of *Thermosynechococcus elongatus* photosystem II: The O_2-evolving enzyme lacking the redox-active tyrosine D, *Biochemistry 43*, 13549−13563.
55. Berthold, D. A., Babcock, G. T., and Yocum, C. F. (1981) A highly resolved, oxygen-evolving photosystem II preparation from spinach thylakoid membranes, *FEBS Lett. 134*, 231−234.
56. Völker, M., Ono, T., Inoue, Y., and Renger, G. (1985) Effect of trypsin on PSII particles. Correlation between Hill activity, Mn-abundance and peptide pattern, *Biochim. Biophys. Acta 806*, 25−34.
57. Arnon, D. I. (1949) Copper enzymes in isolated chloroplasts. Polyphenoloxidase in *Beta vulgaris*, *Plant Physiol. 24*, 1−15.
58. Feyziyev, Y., van Rotterdam, B. J., Bernat, G., and Styring, S. (2003) Electron transfer from cytochrome b_{559} and $tyrosine_D$ to the S_2 and S_3 states of the water oxidizing complex in photosystem II, *Chem. Phys. 294*, 415−431.
59. Rupp, H., Rao, K. K., Hall, D. O., and Cammack, R. (1978) Electron spin relaxation of iron-sulpher proteins studied by microwave power saturation, *Biochim. Biophys. Acta 537*, 255−269.
60. Styring, S., and Rutherford, A. W. (1988) The microwave power saturation of SII_{slow} varies with the redox state of the oxygen-evolving complex in photosystem II, *Biochemistry 27*, 4915−4923.
61. Barry, B. A., and Babcock, G. T. (1987) Tyrosine radicals are involved in the photosynthetic oxygen-evolving system, *Proc. Natl. Acad. Sci. U.S.A 84*, 7099−7103.
62. Un, S., Atta, M., Fontecave, M., and Rutherford, A. W. (1995) *g*-values as a probe of the local protein environment: High-field EPR of tyrosyl radicals in ridonucleotide reductase and photosystem II, *J. Am. Chem. Soc. 117*, 10713−10719.
63. Tracewell, C. A., and Brudvig, G. W. (2003) Two redox-active β-carotene molecules in photosystem II, *Biochemistry 42*, 9127−9136.
64. Faller, P., Rutherford, A. W., and Debus, R. J. (2002) Tyrosine D oxidation at cryogenic temperature in photosystem II, *Biochemistry 41*, 12914−12920.
65. Miller, A.-F., and Brudvig, G. W. (1991) A guide to electron paramagnetic resonance spectroscopy of photosystem II membranes, *Biochim. Biophys. Acta 1056*, 1−18.
66. Dixon, W. T., and Murphy, D. (1976) Determination of the acidity constants of some phenol radical cations by means of electron spin resonance, *J. Chem. Soc., Faraday Trans. 2 72*, 1221−1230.
67. Sahlin, M., Gräslund, A., Ehrenberg, A., and Sjöberg, B.-M. (1982) Structure of the tyrosine radical in bacteriophage T4-induced ribonucleotide reductase, *J. Biol. Chem. 257*, 366−369.
68. Magnuson, A., Berglund, H., Korall, P., Hammarström, L., Åkermark, B., Styring, S., and Sun, L. (1997) Mimicking electron transfer reactions in photosystem II: Synthesis and photochemical characterization of a ruthenium(II) tris(bipyridyl) complex with a covalently linked tyrosine, *J. Am. Chem. Soc. 119*, 10720−10725.
69. Sun, L., Burkitt, M., Tamm, M., Raymond, M. K., Abrahamsson, M., LeGourriérec, D., Frapart, Y., Magnuson, A., Huang Kenéz, P., Brandt, P., Tran, A., Hammarström, L., Styring, S., and Åkermark, B. (1999) Hydrogen-bond promoted intramolecular electron transfer to photogenerated Ru(III): A functional mimic of $tyrosine_Z$ and histidine 190 in photosystem II, *J. Am. Chem. Soc. 121*, 6834−6842.
70. Faller, P., Goussias, C., Rutherford, A. W., and Un, S. (2003) Resolving intermediates in biological proton-coupled electron transfer: A tyrosyl radical prior to proton movement, *Proc. Natl. Acad. Sci. U.S.A. 100*, 8732−8735.
71. Boussac, A., and Rutherford, A. W. (1992) The origin of the split S_3 EPR signal in Ca^{2+}-depleted photosystem II: Histidine versus Tyrosine, *Biochemistry 31*, 7441−7445.
72. Boussac, A., and Rutherford, A. W. (1995) Does the formation of the S_3-state in Ca^{2+}-depleted photsytem II correspond to an oxidation of tyrosine Z detectable by cw-EPR at room temperature? *Biochim. Biophys. Acta 1230*, 195−210.
73. Boussac, A., Sugiura, M., Kirilovsky, D., and Rutherford, A. W. (2005) Near-infrared-induced transitions in the manganese cluster of photosystem II: Action spectra for the S_2 and S_3 redox states, *Plant Cell Physiol. 46*, 837−842.
74. Evelo, R. G., Styring, S., Rutherford, A. W., and Hoff, A. J. (1989) EPR relaxation measurements of photosystem II of S-state oxidation and temperature, *Biochim. Biophys. Acta 973*, 428−442.
75. Faller, P., Pascal, A., and Rutherford, A. W. (2001) β-Carotene redox reactions in photosystem II: Electron transfer pathway, *Biochemistry 40*, 6431−6440.

BI060698E